Electronic structure of ultrathin cobalt films on W(110)

H. Knoppe and E. Bauer
Physikalisches Institut, Technische Universität Clausthal, Leibnizstraße 4, D-3392 Clausthal-Zellerfeld, Federal Republic of Germany
(Received 30 July 1992; revised manuscript received 4 January 1993)

Ultrathin films of cobalt on W(110) are investigated by angle-resolved photoelectron spectroscopy excited with unpolarized and linearly polarized He I radiation. The epitaxial growth of the films is studied by reflection high-energy electron diffraction, x-ray-excited photoelectron diffraction, and Auger electron spectroscopy. The influence of symmetry, packing density, and film thickness on the electronic structure is discussed. The band structure of the quasi-two-dimensional systems is mapped out and compared with full-potential linearized augmented-plane-wave calculations for the pseudomorphic monolayer of Co on W(110) and for the unsupported close-packed monolayer.

I. INTRODUCTION

Ultrathin transition-metal films, that is films with thicknesses up to several monolayers, have attracted increasing interest in recent years, mainly because of their unusual magnetic[1] and chemisorption properties.[2] The fundamental understanding of these properties requires a thorough knowledge of the electronic structure of these layers.

Starting with the pioneering work of Eastman and Grobman,[3] much effort has been devoted during the past 20 years to the understanding of the development of electronic structure from two- to three-dimensional character (for a review, see Ref. 4). Most work on transition-metal overlayers was directed at films on (100) and (111) surfaces of nonmagnetic fcc metals such as Cu, Ag, Au, Pd, and Pt. Except for Pt, the specific surface energies of these substrates are smaller than those of Fe, Co, and Ni so that initial monolayer formation is thermodynamically unfavorable unless encouraged by electronic film-substrate interactions which favor alloying.[5,6] Alloying can be reduced and quasi-two-dimensional initial growth encouraged by deposition at low temperatures, but it would be desirable to grow thermodynamically stable monolayers, which is the case at least for the first layer if refractory metal substrates are used.

The refractory metals W and Mo are suitable substrates from this point of view. They allow us to study the thickness dependence of the electronic structure, the influence of lateral periodicity changes, and also the effect of the symmetry difference between film and substrate in the case of Co and Ni. It has been known for some time that the Ni monolayer on W(110) can grow in pseudomorphic (ps) and close-packed (cp) structures.[7] The growth conditions and the transition between these two structures have been studied in more detail for Ni and Co on Mo(110).[8] This study also showed that below 450 K no agglomeration of the material in excess of one monolayer occurred so that systematic studies as a function of thickness in a quasi-monolayer-by-monolayer growth mode can be made at room temperature. On the basis of these considerations the electronic structure of the system Ni/W(110) has already been studied.[9] Here we report the results of a similar study of the system Co/W(110) for a comparison between fcc and hcp layers. The goal is a better understanding of the relative importance of symmetry, packing density, film-substrate interactions, and film thickness for the evolution of the electronic structure.

II. EXPERIMENTAL PROCEDURE

The experimental setup has been described in detail earlier.[9–11] Therefore, in this work we restrict ourselves to its most important features and to the changes made. The UHV system consists of a VG Instruments, Inc. VG-ESCALAB spectrometer which is connected with a reflection high-energy electron diffraction (RHEED) and preparation chamber. The sample could be transferred in UHV between the two chambers within 10 min. In the course of this study a fast entry air lock was added for an easier exchange of the sample. This required some modifi- cations of the sample holder affecting the liquid-nitrogen cooling of the sample. Therefore, the lowest temperature accessible after this modification was 180 K instead of the 100 K used earlier[9,10] and in part of this work.

The RHEED system was used to determine the structure, the growth mode, and the deposition rate. Details may be found elsewhere.[12] In the RHEED chamber, Co was evaporated from a BeO crucible heated by a tungsten coil and deposited at normal incidence at rates up to 1 monolayer (ML) per minute. During deposition the pressure stayed below 8×10^{-9} Pa.

For photoemission the He I line ($h\nu=21.22$ eV) from a Leybold capillary discharge lamp was used with a home-built triple reflection polarizer,[13] which gave a linear polarization of 90%. For angle-resolved ultraviolet photoelectron spectroscopy (ARUPS) the energy resolution of the analyzer was set to 100 meV without and to 150 meV with polarizer. The angular acceptance was $\pm1°$ for ARUPS and also in the measurement of the angular distribution of the Al $K\alpha$ x-ray-excited photoelectrons. The polar angle of emission of the photoelectrons was changed by rotating the sample. The plane of emission is

0163-1829/93/48(3)/1794(12)/$06.00

identical with the planes of incidence of the UV light and of the x-ray beam. The photon sources were on different sides of the analyzer at polar angles θ of $+36°$ for the He I beam and $-38°$ for the x-ray beam. The sample could also be rotated azimuthally.

For Auger electron spectroscopy (AES) a 1.8-keV, 3-μA electron beam was used. The angular acceptance of the analyzer was generally set at $\pm 12°$. The Auger signal was differentiated by modulation of the target potential with 5 V_{pp} for the detection of impurities and 1 V_{pp} for *in situ* monitoring of the film growth. In the spectrometer chamber Co was evaporated from a 10-mm-long and 5-mm-diameter high-purity Co cylinder with a tight-fitting 2-mm coaxial ceramic tube inside, which was resistively heated by a tungsten coil. After careful outgassing a working pressure of less than 6×10^{-9} Pa was reached at deposition rates of about 0.1 ML/min. The contamination of the Co films by the residual gas was faster than for Ni,[9] allowing measurement periods of only 3 h without noticeable influence on the ARUPS spectra.

The Co films generally were annealed for 1 min at about 700 K up to and at 450 K above 1.0-ML coverage in order to improve the order of the films without danger of agglomeration.[8,14] This resulted in sharper ARUPS features.

III. RESULTS

A. Structural characterization

RHEED intensity oscillations (Fig. 1) indicate quasi-monolayer-by-monolayer growth of cobalt on W(110). On the basis of simultaneous measurements with a quartz-crystal microbalance[12] the constant period after the third maximum is attributed to a film thickness of 1 ML with the density of the bulk layer material. The damping of the oscillations depends not only on temperature, but also on the background pressure and the cleanliness of the source as found for other materials.[12] The larger damping in the room-temperature deposition [Fig. 1(a)] is due to a faster approach to the steady state of terraces and steps. At 100 K [Fig. 1(b)] the nucleation rate is higher and the diffusion length smaller, so that the surface becomes rough on an atomic scale. However, the film can be smoothed by annealing (see Sec. II).

The RHEED pattern shows the slightly broadened substrate reflexes with little diffuse background intensity up to a coverage of 0.7 ML. Then an eightfold superstructure along the [001] azimuth appears as reported by other authors,[14,15] but the periodicity changes to about 7.2-fold at 1.0 ML. For the closely related Co/Mo(110) system the same superstructures were found.[8] Along $[1\bar{1}0]$ the periodicity of the substrate is maintained.

We conclude that initially a low-density pseudomorphic bcc(110) monolayer is formed. Upon further Co deposition the packing density increases by a factor of 9.2/7.2 along $[001]_W$, but is maintained along $[1\bar{1}0]_W$ so that a monolayer with approximate hcp structure is formed. It is compressed by 1.2% in the $[001]_W$ direction and is dilated by 3.1% along $[1\bar{1}0]_W$ with respect to the bulk Co(0001) plane.

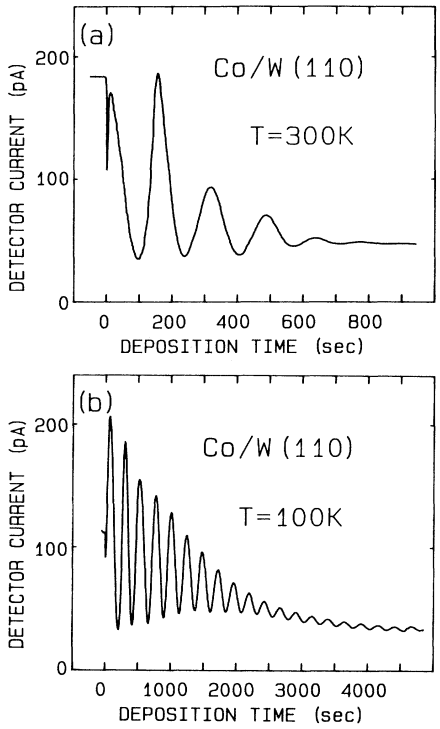

FIG. 1. Intensity oscillations of the specular RHEED beam during growth of Co on W(110) at room temperature (a) and at 100 K (b) with the $[1\bar{1}0]$ azimuth in the plane of incidence. The primary energy was 15 keV, the glancing angles were 0.36° (a) and 0.33° (b). Note that the time scales are different.

With further increasing coverage the superstructure reflexes weaken and disappear completely at about 4 ML, leaving a hexagonal pattern with the bulk lattice spacing of Co(0001). Within our limits of error it is not clear at what stage of epitaxy the distortion of the hexagonal layers vanishes. The final configuration consists of a misfit vernier ($[001]_W$) and of misfit dislocations ($[1\bar{1}0]_W$).[5] The orientation of the layers corresponds to the Nishiyama-Wassermann orientation of fcc crystals with $(0001)_{Co}\|(110)_W$ and $[11\bar{2}0]_{Co}\|[001]_W$. The atoms in the second layer can be located in two different equivalent sites which causes twinning of the epitaxial film. The following layers grow, therefore, in two differently orientated domains with the natural hcp structure.

The hcp structure is confirmed by the angular distribution of the core-level photoelectrons, which is sensitive to the local crystalline order of the outermost atomic layers and allows us to distinguish between hcp and fcc stacking of close-packed layers.[16] This is a result of forward focusing along close-packed rows of atoms which was calculated recently for Co $2p_{3/2}$ photoelectrons excited with AlK_α radiation ($E_{kin}=703$ eV) in a slab of Co(0001).[17] Therefore we probed the direction sensitive to the stacking sequence with polar angle scans for layers of 7 ML [Fig. 2(a)] and 12 ML. The intensity asymmetry about the normal emission is an effect of the changing angle of incidence of the x-ray beam: at 52° the beam is incident parallel to the surface. At $-12°$ the rotation of the sam-

ple was mechanically limited. The smoothed background at 800 eV kinetic energy [Fig. 2(a)] was multiplied by a constant factor and then subtracted. The result is shown in Fig. 2(b) together with the calculated polar scan[18] for the $\phi=90°$ azimuth of step-averaged Co(0001).[17] Because of twinning and because of monoatomic steps, both domains with C_{3v} symmetry are present which gives macroscopically a C_{6v} symmetry for the growing Co film. Intensity differences between the two curves are due in part to the different geometry in the calculations.[17] The experimental curve has two main structures centered at 0° and 35° separated by a minimum at 15°. The calculations yield a minimum at 20°, but there is rather good agreement for the peaks at 0°, 9°, 30°, 35°, and 43°. The theoretically predicted peak at 57° is suppressed by the glancing incidence of the x-ray beam.

The deposition rate of the evaporator in the analyzer chamber was calibrated to the RHEED coverage scale by AES in the following manner: A Co layer of 0.80 ML, which showed the eightfold superstructure, was prepared in the RHEED chamber and transferred *in vacuo* to the analyzer chamber in which the Co deposition was continued with *in situ* monitoring of the AES signal. The upper of the two curves in Fig. 3 taken at normal emission shows the development of the differentiated Co $M_{2,3}M_{4,5}M_{4,5}$ Auger-electron signal obtained in this manner. It was multiplied by a constant factor in order to separate it from the curves obtained by continuous

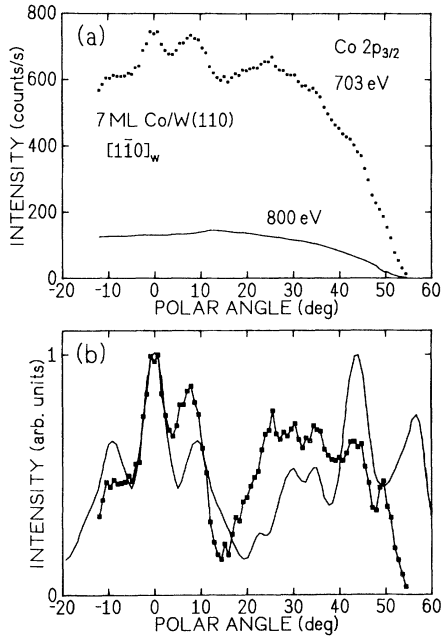

FIG. 2. (a) Polar scan of the Al $K\alpha$ radiation excited Co $2p_{3/2}$ photoelectron distribution ($E_{kin}=703$ eV) from a film of 7-ML Co on W(110) in the [11$\bar{0}$] azimuth of tungsten (upper curve; count time 15 s per data point) and smoothed background at $E_{kin}=800$ eV (lower curve). (b) Calculated polar scan (solid curve, Ref. 18) for step-averaged Co(0001) in the $\phi=90°$ azimuth (Ref. 17) compared with the data of (a) after background subtraction (curve with data points).

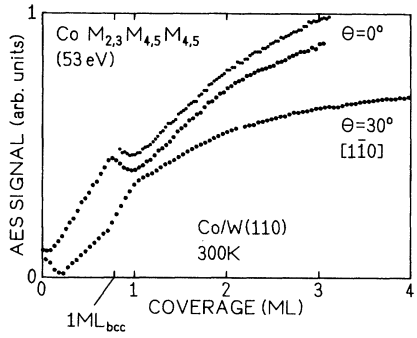

FIG. 3. Differentiated intensity of the Co $M_{2,3}M_{4,5}M_{4,5}$ Auger electrons ($E=53$ eV) during growth of Co on W(110) at room temperature. The curves were taken at normal emission ($\theta=0°$) and at 30° off normal in the [1$\bar{1}$0] azimuth. The topmost curve was taken after 0.80-ML Co were deposited in the RHEED chamber, see text. Continuous recording.

deposition from the beginning in the analyzer chamber. The maximum possible ps coverage of 0.78 ML is marked by 1 ML_{bcc}. At room temperature the curve breaks that indicate the onset of the ps-to-cp monolayer transition are always found at somewhat smaller coverages. Details on the nature of this transition are given elsewhere.[7,8,19,20] The polar angles 0° and 30° were chosen in contrast to the more usual value of 42° for spectroscopy with cylindrical mirror analyzers,[8,14] because detailed measurements show[10,11] that at 42° the sensitivity to the ps-to-cp layer transition is rather poor. The differences are due to the influence of backscattering of low-energy Auger electrons in angle-resolved spectroscopy. Thus, in Fig. 3, the maximum at 1 ML_{bcc} for 0° is caused by increased backscattering of Auger electrons from Co atoms in substrate lattice site positions by the substrate. Lineshape changes can also lead to slope changes in AES curves,[21] but these are expected to depend little upon emission angle, in contrast to the 30° curve in Fig. 3 which has a quite different coverage dependence. Another prerequisite for sharp slope changes at the structural transitions is contamination-free deposition as stated above. During the growth of the following layers the Co signal increases monotonically with rounded slope changes close to integer monolayers, indicating the start of a new monolayer before the completion of the preceding layer.

B. Normal emission ARUPS

An overview of the evolution of electronic structure with increasing coverage is given in Fig. 4. Here, cobalt was deposited cumulatively at room temperature in doses of 0.206 ML, exceptionally without annealing. At the bottom the ultraviolet photoemission spectroscopy (UPS) spectrum of clean W(110) is shown. The other spectra are shifted vertically for clarity. The sharp monolayer peak close to the Fermi level (E_F) at 0 eV shifts only a little to a higher binding energy (E_B) during the transition to the cp monolayer and is visible up to 2.5 ML. During the growth of the second and third monolayer broader

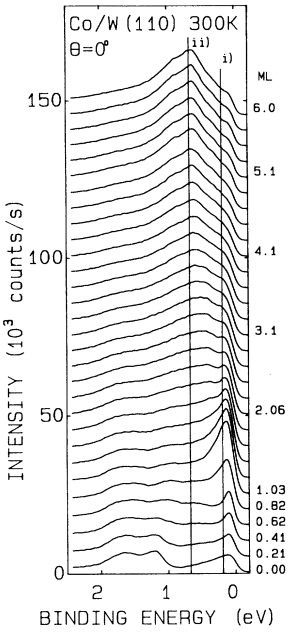

FIG. 4. Normal emission ARUPS spectra of Co/W(110) as a function of coverage at room temperature, excited with unpolarized He I light. The first curve is from the clean tungsten surface, the others are shifted for clarity. The parameter is the thickness in hcp monolayers (ML). The lines i) and ii) indicate the energies at which the data of Fig. 5 were measured.

structures at higher E_B develop and increase in intensity. At 4 ML the peak shape characteristic of thicker films is reached, except for the surface-state emission at $E_B=0.3$ eV,[22] which is weak at $h\nu=21$ eV and becomes detectable as a small shoulder only above 4.8 ML.

The evolution of the intensities at the energies marked by lines i) and ii) in Fig. 4 during continuous Co deposition is shown in Fig. 5. Curve i) taken at $E_B=0.19$ eV close to the monolayer peak clearly shows the effect of the structural transition whereas curve ii) at 0.67 eV shows the bulk band intensity and is rather insensitive to the structural change. Linear segments within the curves

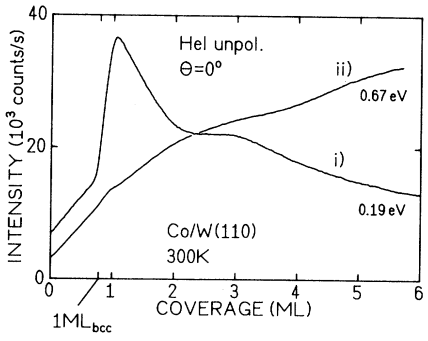

FIG. 5. Electron spectroscopic signals in normal emission geometry during deposition of Co on W(110) at room temperature obtained with unpolarized He I radiation. The binding energies of curves i) (0.19 eV) and ii) (0.67 eV) are marked in Fig. 4. Continuous recording.

indicate approximate layer-by-layer growth. As in Fig. 3 the rounded transitions are due to deposited atoms which are no longer incorporated and already start the growth of the next layer, because, even at room temperature, the diffusion length is limited. The especially large rounding at the transition from the second to the third layer is due to the fact that the layer wants to grow in the Stranski-Krastanov mode but is kinetically limited to do so.[8] The subsequent growth is dominated by Co-Co interactions and, therefore, is more homoepitaxylike which favors Frank–van der Merwe-type growth.

Normal emission spectra, excited with He I light, linearly polarized parallel (p) or normal (s) to the plane of incidence of the light, are shown on the left- and right-hand side, respectively, of Fig. 6. Assuming, as usual, total symmetric final states, we have even and odd initial states with respect to the mirror plane containing the $[1\bar{1}0]_W$ azimuth in this case, excited with p- and s-polarized light, respectively. The components of the vector potential **A** are given with respect to the $[001]_W$ azimuth as the x direction, z is normal to the surface.

The lower part of Fig. 6 shows the spectra of the substrate, of the ps and cp monolayer and double layer, and the upper part shows spectra of thicker layers. The Co films have been annealed (see Sec. II). The sharp peak of the left bcc monolayer spectrum (0.7 ML) is very close to the Fermi level. At 1.0 ML the peak position of this even state is shifted somewhat from E_F and its intensity has increased significantly. The monolayer spectra excited with s-polarized light react very differently to the ps-to-cp transition. The rather broad band of the ps layer at

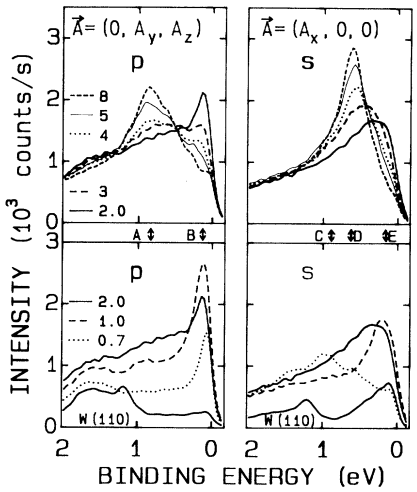

FIG. 6. Normal emission ARUPS spectra as a function of Co coverage on W(110), excited with polarized He I light. The $[1\bar{1}0]_W$ azimuth is in the plane of incidence of the light. The lower parts of the figure show the spectra from clean W(110), from the bcc and hcp monolayers (0.7 and 1.0 ML) and from the double layer (2.0 ML). The upper parts show the spectra from 2.0 to 8 ML of Co. The components of the vector potential **A** are given for the left and right panel (p and s polarization) ($x \| [001]_W$, $y \| [1\bar{1}0]_W$, z normal to surface). The Co films have been annealed at 700 K up to and at 450 K above 1.0 ML. At the energies $A-E$ the data in Fig. 7 were measured.

$E_B = 0.95$ eV vanishes and a new peak appears at 0.19 eV for 1.0 ML.

With increasing film thickness the sharp even band (p-polarized light) at the Fermi edge vanishes at more than 3 ML and the even bulk band at $E_B = 0.85$ eV begins to form. The odd double-layer band is rather broad (Fig. 6, right side) and changes into the bulk band at 0.64 eV dominating the unpolarized spectra.

Rotating the sample azimuthally by 90° and exchanging p and s polarization yields almost the same spectra, which shows that the corresponding states are excited by the A_x or the A_y components. Only the rather weak structure at 0.95 eV for 1.0 ML (Fig. 6, left side) becomes visible then for both polarizations, which means that this structure consists of two components. One is excited by the A_y part and the other by the A_z part of the vector potential. The latter is also responsible for the excitation of the 0.3-eV surface state belonging to the total symmetric representation.[23] It is visible weakly in the upper left part of Fig. 6 for 5 and 8 ML.

Figure 7 shows the intensities at selected energies versus coverage in normal emission comparable to Fig. 5 but excited with polarized light with the $[001]_W$ azimuth in the plane of incidence. The energy positions of curves A to E of Fig. 7 are marked in Fig. 6 for the corresponding A_x and A_y light vector components. Curves A and B in Fig. 7(a) are, in general, similar to those of Fig. 5 taken with unpolarized light but, unlike curve i) in Fig. 5, curve B has an almost constant slope between 2 and 5 ML and curve A is more sensitive to the structural transition than curve ii) in Fig. 5. The response of the intensities in Fig. 7(b) to the change of the monolayer structure is quite different. During ps growth curve E taken at 0.17 eV even decreases and then sharply increases as the cp structure starts to form. In contrast to curve B at similar energy it has a clear maximum at 3 ML. Curve C peaks at the bcc monolayer and has a minimum at 1.0 ML. D was taken close to the dominating bulk peak and decreases slightly from 0.7 to 1.0 ML.

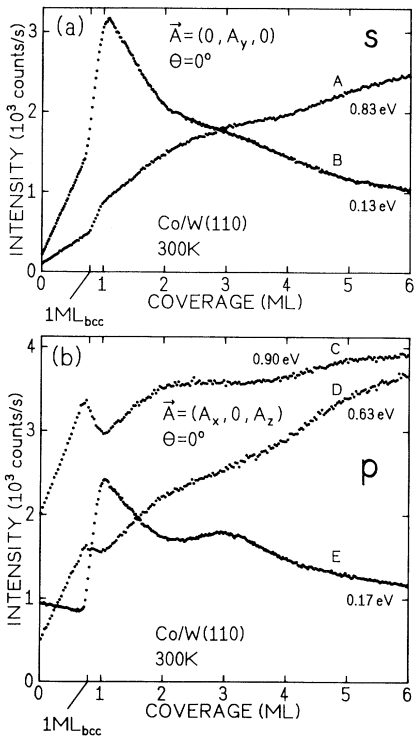

FIG. 7. Same as Fig. 5, but using polarized light with the $[001]_W$ azimuth in the plane of incidence of the light. The components of the vector potential **A** are given for (a) and (b) (s and p polarization). The curves A–E were taken at the indicated energies, which are also marked in Fig. 6. Curve C was shifted vertically by 1500 counts/s for clarity.

Summarizing, we find similar intensity changes at coverages above 1 ML for curves A and D, but different signs of slope at the 0.7-ML ps-cp transition explaining the insensitivity to the structural change of curve ii) in Fig. 5 taken with unpolarized light. The intensities closer to the Fermi level (curves B and E in Fig. 7) very clearly show the effect of the structural change beginning at 0.7 ML. Also, despite the lower intensity, the linear segments due to the layer-by-layer growth are better resolved in the measurements with polarized light.

C. Off-Normal photoemission spectra

In order to obtain the $k_{\parallel}$ dependence of the energy bands of the Co layers (see below), ARUPS scans with the polar angle as parameter were made for coverages from 0.6 to 12 ML. The energy range 0–5 eV binding energy was studied, but characteristic Co bands were found only from E_F to 2 eV. Many series of spectra were taken using unpolarized light, but polarized light was used also in order to resolve even and odd symmetry bands with respect to the two mirror planes of the W(110) substrate.

For convenience, the film thickness was determined using the changes of the ARUPS intensities shown above. That this method can also yield valuable information in off-normal geometry is illustrated in Fig. 8 at the polar angle $\theta = 30°$ along $[001]_W$ for p-polarized light. The pronounced peak at 0.7-ML coverage is caused by an even state which is characteristic for the ps monolayer. This state is visible in Fig. 9(a) close to E_F. Figure 9 was taken

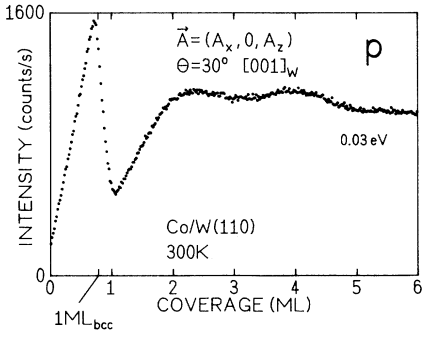

FIG. 8. Same as Fig. 7 but with the sample rotated 30° off normal in the $[001]_W$ azimuth using p-polarized light; $E_B = 0.03$ eV.

with unpolarized light and shows the ARUPS spectra of the clean substrate and for Co coverages of 0.7, 1.0, and 2.0 ML at $\theta=30°$ (a) and 51° (b) in the $[001]_W$ direction. In this azimuth the ps monolayer (0.7 ML) has sharper features close to E_F than the cp monolayer (1.0 ML). At higher E_B the intensity of the W bands at 2.0, 3.2, and 4.3 eV decrease with Co coverage, as expected. At 30° (a) the Co intensity increases in the energy range shown so strongly with increasing coverage that the 2.0- and 3.2-eV W signals appear to increase. This shows that measurements at only one energy can easily lead to misinterpretations.

Annealing of the monolayers up to 700 K was found to have a large influence on the sharpness of the Co bands, in particular at 1 $ML_{bcc} \simeq 0.78$ ML due to the coexistence of the ps and cp structures at room temperature.[7,8,19] For coverages above 1.0 ML care had to be taken not to exceed 450 to 500 K to avoid the formation of three-dimensional crystals.[8,14] Figure 10 shows the influence of the annealing and measurement temperature on the series of polar angle-dependent spectra taken with unpolarized light with the $[1\bar{1}0]_W$ azimuth in the plane of emission. The polar angle θ is given on the right-hand side for every third spectrum.

Figure 10(a) shows the effect of annealing at 450 K on the spectra of the double layer. The band splitting between 30° and 60° is observed in a similar manner up to the highest coverages studied. The intensity of the lower band dominating before annealing is reduced and the intensity of the upper band closer to E_F increased, but no change of the binding energies is observed. As a result of the improvement of order, the bands are much better resolved.

For a proper comparison with calculated band structures the possibility of indirect transitions has to be taken into account. Therefore, we also checked the influence of cooling of the sample. Figure 10(b) shows the spectra from a 12-ML film taken at 300 and 180 K. The intensities of all bands were found reversibly to be higher at 180 K. In particular, the band at the Fermi level around 0° sharpens considerably upon cooling.

Other noteworthy features are (i) an apparent asymmetry with respect to normal emission of the sharp peaks seen with p-polarized light in Fig. 6 for 0.7, 1.0, and 2.0 ML [compare the spectra for −7.6° and +7.4° in Fig. 10(a)]. Additional measurements with linearly polarized light and smaller polar angle increments revealed satis-

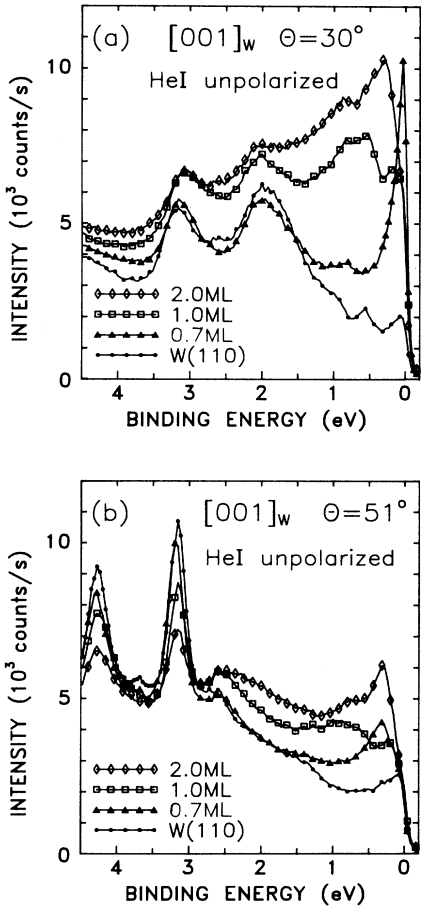

FIG. 9. Off-normal emission ARUPS with the $[001]_W$ azimuth in the plane of electron emission at polar angles of 30° (a) and 51° (b). The spectra were taken with unpolarized He I light from the clean W(110) substrate and for selected coverages of Co. The films have been annealed at 700 K (0.7 and 1.0 ML) and 450 K (2.0 ML).

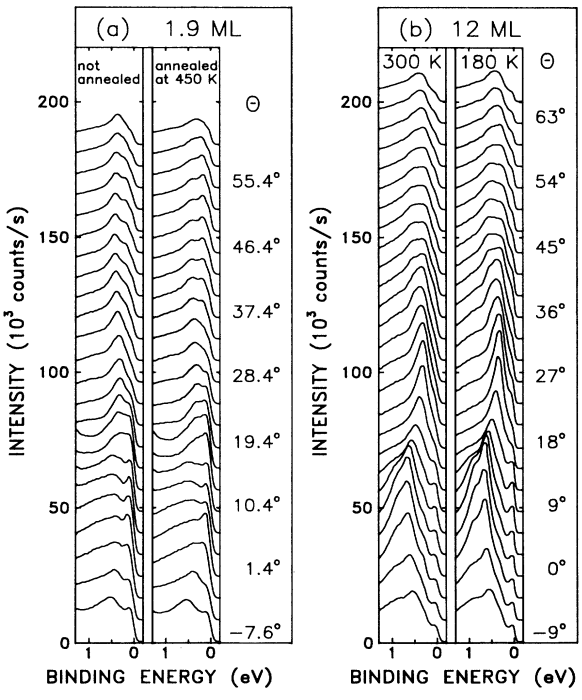

FIG. 10. Angular-dependent ARUPS scans with the $[1\bar{1}0]_W$ azimuth in the plane of emission. The curves are shifted for clarity. The parameter is the polar angle in degrees. (a) shows the effect of annealing at 450 K on the spectra of a 1.9-ML-thick Co film; (b) compares the spectra of a 12-ML-thick Co film taken at room temperature and at 180 K.

factory mirror symmetry about 0° of the peak positions, but not of the intensities. The even bands are intense in a small angular range at negative polar angles. The same unexpected strong influence of the angle of incidence of the light was observed in the Cu/W(110) system.[10]

D. Two-dimensional band structures

The parallel component of momentum of the initial electronic states is given by the polar angle of emission θ and the kinetic energy of the electron in vacuum,

$$k_{\parallel}=\sin(\theta)[(2m/\hbar^2)E_{\rm kin}]^{1/2} .$$

Assuming $k_{\parallel}$ conservation during the photoemission process, this formula gives the momentum of purely two-dimensional initial states.

The Co-induced bands of the ps monolayer are mapped out in Fig. 11 where the peak positions of the spectra taken with polarized light plotted against the absolute value of $k_{\parallel}$ for the [001] and the $[1\bar{1}0]$ azimuth. Even and odd initial states with respect to the corresponding mirror planes are marked by crosses and circles, respectively. As mentioned in Sec. III B these states are excited by *p*- and *s*-polarized light, respectively. Thus, when the mirror plane is changed by turning the sample, the bands that change their parity at $k_{\parallel}=0$ have crosses on one side and circles on the other side of $\bar{\Gamma}$ in Fig. 11. The data measured with unpolarized light yield no additional information here. The inset shows the bcc(110) surface Brillouin zone. In the repeated zone scheme there is mirror symmetry with respect to the first zone boundary in the $[1\bar{1}0]$ azimuth at $\bar{N}$ only; along [001] beyond $\bar{H}$ the point $\bar{N}$ is reached again.

At the $\bar{\Gamma}$ point the bands 1 and 2*b* dominate the spectra, while band 2*a* is a weak feature with the same parity as band 2*b*. Along $\bar{\Gamma}\bar{N}$ band 1 is even (crosses) with parabolalike dispersion, and along $\bar{\Gamma}\bar{H}$ it is odd (circles) and exactly flat at E_F. This is a hint that its true energy position lies probably above the Fermi level (compare the sharpness and position of the corresponding peak in Fig. 6, bottom left for 0.7 ML). In between $\bar{\Gamma}$ and $\bar{H}$ close to E_F is the intense even band (crosses) which caused the sharp maximum at the coverage 0.7 ML in Fig. 8 and was shown in Fig. 9(a). The polar angle $\theta=30°$ therein corresponds to $k_{\parallel}=1.0$ Å^{-1}. Figure 9(b) ($\theta=51°$) shows the odd band at 1.6 Å^{-1} between $\bar{H}$ and $\bar{N}$. Along $[1\bar{1}0]$ the even states close above band 1 and the two bands around $\bar{N}$ are rather weak features in the spectra.

Figure 12 shows the band mapping for the cp monolayer. The surface Brillouin zone of the Co(0001) plane and its azimuthal orientation with respect to the substrate are shown in the inset. Band 1 is comparable to band 1 of the ps structure in Fig. 11, with slightly lower energy at $\bar{\Gamma}$ and enlarged dispersion in the $[1\bar{1}0]_W$ direction. The most striking feature in the spectra of the cp monolayer is an intense odd band at all polar angles along the $[1\bar{1}0]_W$ azimuth, which appears throughout the whole Brillouin zone along $\bar{\Gamma}\bar{M}$ in Fig. 12 (right side, band 2, circles). Band 2 is even with large dispersion along $[001]_W$ (crosses) and odd along $[1\bar{1}0]_W$ (circles) where it crosses band 1 and a weaker second even band close to $\bar{\Gamma}$.

At about the same energy position as band 2*b* for 0.7 ML (Fig. 11), weak states are found for 1.0 ML (bands 3 and 4, Fig. 12), but the parities are different, compare Fig. 6 and Sec. III B. Completely new are two even parabolalike bands that are approximately symmetric to $\bar{M}$, which are also weak in the spectra. Therefore, data points taken with unpolarized light (dots) are added in Fig. 12. Closer inspection reveals that the symmetry center of these bands corresponds rather to the $\bar{N}$ point of the bcc(110) structure. This is consistent with the unchanged packing density of the slightly distorted hexagonal Co monolayer in the $[1\bar{1}0]_W$ azimuth which was mentioned in Sec. III A. Along the $[001]_W$ azimuth we find several new states which are rather broad features in the spectra (compare Fig. 9). In this direction the large change in packing density is clearly reflected by the even band (crosses) at point $\bar{K}$.

The growth of the second atomic layer with hexagonal symmetry influences the electronic structure strongly. In Fig. 13 the data for 2.3 ML in the $[1\bar{1}0]_W$ azimuth converted to $E(k_{\parallel})$ are shown. At this coverage the intensity asymmetry with respect to normal emission mentioned

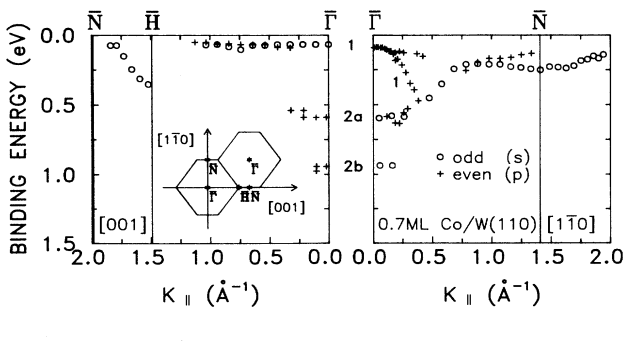

FIG. 11. Band mapping of the pseudomorphic monolayer (0.7 ML) of Co/W(110). Crosses and circles indicate data points obtained with *p*- and *s*-polarized light, respectively. The band numbers refer to Table I. The inset shows the surface Brillouin zone of W(110).

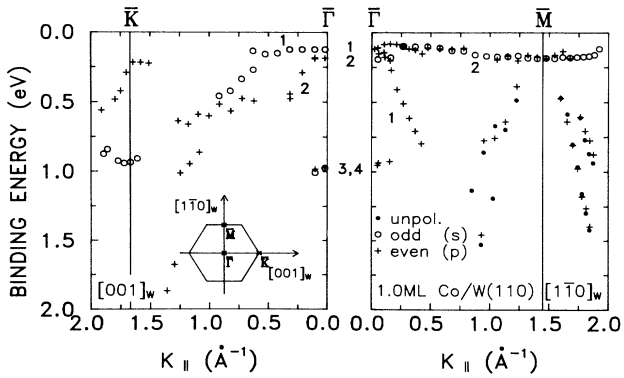

FIG. 12. Same as Fig. 11 but for the hexagonal monolayer (1.0 ML). Data points from measurements with unpolarized light dots) are included for the parabolalike bands at $\bar{M}$. The inset shows the surface Brillouin zone of the Co(0001) plane.

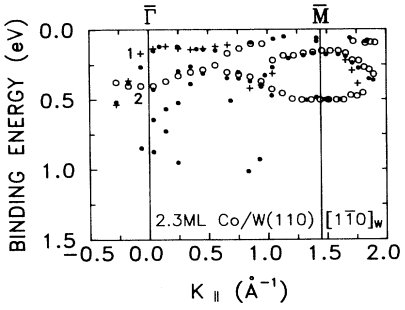

FIG. 13. Band mapping of the 2.3-ML-thick Co film in the $[1\bar{1}0]_W$ azimuth. Negative $k_\parallel$ values correspond to negative polar angles (see text). The symbols are the same as in Figs. 11 and 12.

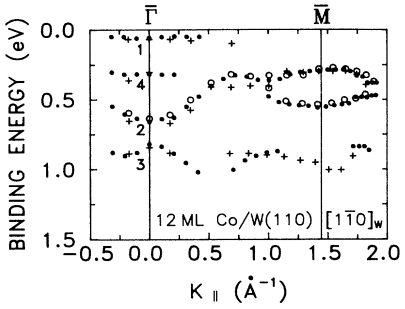

FIG. 14. Same as Fig. 13 but for a 12-ML-thick Co film.

above is still present, compare Fig. 10(a) for 1.9 ML. The even band 1 with large dispersion (crosses), which is strong only at negative polar angles corresponding to negative $k_\parallel$ values in Fig. 13, and the second flat even band between 0 and 0.7 Å^{-1} are similar to the even monolayer bands close to E_F (Figs. 11 and 12). The odd band 2 at $\bar{\Gamma}$, instead, has considerably lower energy and splits at about 1 Å^{-1} in the double layer. The odd states (circles) closest to E_F are observed only at coverages exceeding 2.0 ML and are sharpest at 2.9 ML.

For comparison, the $k_\parallel$ dependence of the photoemission features of a 12-ML-thick Co film is shown in Fig. 14. At this thickness the band structure is already three dimensional so that $E(k_\parallel)$ does not represent a physically meaningful dispersion relationship. Yet, the split odd bands at $\bar{M}$ are very similar to those shown in the previous figure. The band 4 at $E_B = 0.3$ eV around $\bar{\Gamma}$ is attributed to the bulk surface state.

IV. DISCUSSION

We start with a symmetry analysis of the Co bands at the $\bar{\Gamma}$ point following the method described earlier.[9,10] As mentioned in Sec. III B all strong Co-induced states detected at $\theta = 0°$ have different parities with respect to the two mirror planes of the W(110) substrate. Thus, the observed bands are d_{xz}- and d_{yz}-like at $\bar{\Gamma}$, except for the bulk surface state at 0.3 eV (Ref. 22) and the feature at 1 eV for 1.0 ML, which are $d_{3z^2-r^2}$-like. Electric-dipole transitions in normal emission geometry from $d_{x^2-y^2}$- and d_{xy}-like states cannot be observed.[23] Table I lists the binding energies E_B at $\bar{\Gamma}$ (referred to E_F) for characteristic coverages. The band number was chosen in a way to allow for a comparison of states with the same orbital character.

Recently, in a study of the Cu on W(110) system, states with strong interfacial character were discerned from those with pure overlayer localization by their intensity decrease with increasing coverage in connection with band-structure calculations.[24] For Co on W(110) the situation is more complicated because the structural transition, which occurs for Cu in the double layer,[10] occurs already in the monolayer. The change from twofold to sixfold symmetry certainly has a strong influence on possible interface states of the pseudomorphic Co layer on W(110) as will be shown in the following. For hexagonal Co on W(110) the formation of interface states is rather unlikely due to the disturbance by the incommensurability with 7.2-fold periodicity along $[001]_W$.

One candidate for an interface state with nearly unchanged energy and decreasing intensity from 1 to 3 ML is band 1 (Table I, Fig. 6, left side). But for 1.0 ML it can be explained by a Co layer band (see below).

A. The pseudomorphic monolayer

In order to assess the influence of symmetry, packing density, film-substrate interaction, and film thickness on the electronic structure a comparison with reliable band-structure calculations is very helpful. For the bcc monolayer (0.7 ML) of Co on W(110) these were performed by Weimert, Noffke, and Fritsche[25] using the full-potential linearized augmented-plane-wave (FLAPW) method.[26]

TABLE I. Coverage dependence of the binding energies (in eV) of the Co states at $\bar{\Gamma}$. The band number refers to Figs. 11–14, the orbital character is given with respect to the x coordinate parallel to the $[001]_W$ direction and z normal to the surface. The true energy positions of the states marked by an asterisk are possibly above E_F.

Band number		Coverage (ML) 0.7	1.0	2.0	3.0	4	7	12
1	d_{yz}	0.08*	0.12	0.14	0.17		0.07*	0.07*
2	d_{xz}	(a) 0.60,(b) 0.95	0.19	0.39	0.47	0.57	0.59	0.64
3	d_{yz}		0.95		0.73	0.84	0.86	0.85
4	$d_{3z^2-r^2}$		1.00				0.3	0.3

Their sample consists of a slab of five W(110) layers with one pseudomorphic Co layer on each side. The Co atoms at W lattice sites were relaxed vertically by 0.21 Å according to their smaller size.

Figure 15 shows the FLAPW-calculated spin-resolved Co bands.[25] The majority (spin-up, triangles) and minority (spin-down, squares) states with more than 80% and 60% localization within the Co layer (filled and open symbols, respectively) were selected to allow for a comparison with the measured bands mapped out in Fig. 11. In Table II the binding energies of the calculated states are compared with the measured data for the ps monolayer at $\bar{\Gamma}$, $\bar{N}$, and $\bar{H}$. States with more than 80% localization within the Co layer are underlined, those with less than 60% are given in parentheses. The calculations generally yield symmetric (s) and antisymmetric states (a) with respect to the center plane of the slab. The deviations between their energies increase with decreasing surface localization. This is connected with the fact that only purely two-dimensional electronic states are described well by $k_{\parallel}$.

At $\bar{\Gamma}$ the Co minority bands ($\downarrow$) with $d_{x^2-y^2}$ and d_{yz} character are found somewhat above the Fermi level. The d_{yz} state is observed in the normal emission spectra (Fig. 6, left side, 0.7 ML) directly at E_F, so that the experimental binding energy is uncertain, but the large dispersion of band 1 (Fig. 15) below E_F from $\bar{\Gamma}$ to $\bar{N}$ agrees quite well with the measurements (Fig. 11, band 1). Along $\bar{\Gamma}\bar{H}$ this band 1 (Fig. 11) is odd and stays exactly at E_F until it decreases in intensity at about 0.5 Å^{-1}. At about the same $k_{\parallel}$ value the odd calculated states lose their Co localization and disperse to higher E_B.

The $d_{x^2-y^2,\downarrow}$ band above E_F increases in energy along $\bar{\Gamma}\bar{H}$ beyond 0.5 Å^{-1} (Fig. 15). Between about 0.3 and 1 Å^{-1} it can be correlated with the intense even band along

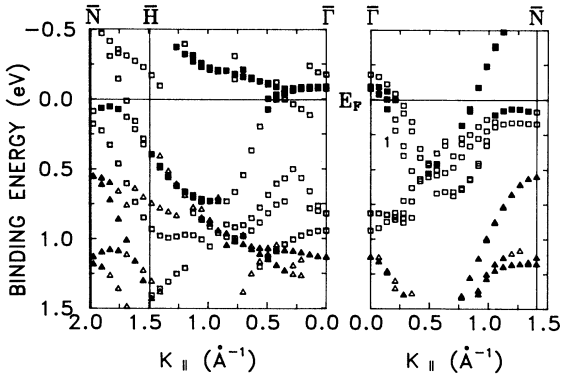

FIG. 15. Calculated spin-resolved band structure (Ref. 25) for one pseudomorphic, vertically relaxed Co layer on each side of a slab of five W(110) layers. Triangles and squares denote majority (spin-up) and minority (spin-down) states, respectively, which are localized with more than 80% (full symbols) and 60% (open symbols) within the Co.

[001] at E_F [Figs. 11 and 9(a)]. The weak even states above band 1 along [1$\bar{1}$0] (Fig. 11, $k_{\parallel} < 0.5$ Å^{-1}) can be explained by the same $d_{x^2-y^2,\downarrow}$ band. As mentioned before, states with this character cannot be observed in normal emission geometry, that is at $\bar{\Gamma}$.

The majority band $d_{yz,\uparrow}$ 1.2-eV below $d_{yz,\downarrow}$ is localized in the Co layer with almost 100% at $\bar{\Gamma}$ only (Fig. 15). For finite $k_{\parallel}$ values the Co localization rapidly decreases as a result of interaction with W states. As shown in Fig. 6 states with d_{yz} symmetry at $\bar{\Gamma}$ are not observed around $E_B = 1$ eV in experiment.

Because of its symmetry the strong d_{xz}-like peak at $E_B = 0.95$ eV (Fig. 6, right side, 0.7 ML) can be identified

TABLE II. Comparison of theoretical (Ref. 25) and experimental binding energies (in eV) of spin-up ($\uparrow$) and spin-down ($\downarrow$) states of the bcc Co monolayer on W(110) (0.7 ML) at $\bar{\Gamma}$, $\bar{N}$, and $\bar{H}$. The calculated states listed here have more than 60% surface localization and are also shown in Fig. 15, except for $d_{xz,\downarrow}$ at $\bar{\Gamma}$ (47%, in parentheses). The E_B values of the states with more than 80% localization are underlined. The predominant orbital character is given. s and a refer to symmetric and antisymmetric states with respect to the center plane of the CoW_5Co slab. (For E_B marked by an asterisk, compare Table I.)

$\bar{\Gamma}_{calc}$		$d_{x^2-y^2,\downarrow}$	$d_{yz,\downarrow}$	$d_{3z^2-r^2,\downarrow}$	$(d_{xz,\downarrow})$	$d_{xy,\downarrow}$	$d_{yz,\uparrow}$
	s	−0.094	−0.079	0.814	(0.863)	(0.877)	1.125
	a	−0.179	−0.079	0.814	(1.042)	(0.939)	1.126
$\bar{\Gamma}_{expt}$			d_{yz}		d_{xz}		
			0.08*		0.60, 0.95		
$\bar{N}_{calc}$		$d_{3z^2-r^2,\downarrow}$		$d_{xy,\uparrow}$	$d_{3z^2-r,^2\uparrow}$		
	s	0.087		0.546	1.129		
	a	0.173		0.546	1.175		
$\bar{N}_{expt}$		even	odd				
		0.12	0.25				
$\bar{H}_{calc}$		$d_{3z^2-r^2,\downarrow}$	$d_{xy,\downarrow}$	$d_{x^2-y^2,\downarrow}$		$d_{3z^2-r^2,\uparrow}$	$d_{xy,\uparrow}$
	s	0.438	0.374	1.406		1.300	
	a	−0.173	0.392	0.928		0.741	1.426
$\bar{H}_{expt}$			odd				
			0.36				

as the minority $d_{xz,\downarrow}$ state with only 47% Co localization (Table II, not included in Fig. 15), but with a localization of 26% in the top W layer. Thus, this state is rather an interface than a Co monolayer state. It can be interpreted as being hybridized with the W-5d bands. (Compare the energetic positions of the W features in Fig. 6.) The nature of the weaker feature at $E_B = 0.60$ eV is not obvious.

The intensity is strongly enhanced also below 1 eV in Fig. 6, right side, for 0.7 ML. This is possibly due to interface states or a Co-induced enhancement of substrate bulk states, which should be checked with a tunable light source. A hint for the interfacial character of the d_{xz} state at $E_B = 0.95$ eV is its disappearance upon the transition to hexagonal symmetry.

At the Brillouin-zone edges $\bar{N}$ and $\bar{H}$ two bands agree with minority states (see Table II), but the odd band at $\bar{N}$ cannot be explained by calculated states of similar dispersion and the same parity.

B. The hexagonal monolayer

To our knowledge band-structure calculations for hcp Co monolayer systems have been performed only for the unsupported monolayer. The relevant parts of the nonspin-polarized band structure obtained by Wimmer[27] with the FLAPW method have been replotted in Fig. 16 in the scale of Fig. 12 for better comparison. The orbital character of the states at $\bar{\Gamma}$ from bottom to top is $d_{3z^2-r^2}$, $d_{x^2-y^2}$ and d_{xy} (degenerated), d_{xz} and d_{yz} (degenerated). Quantitative agreement with the experimental data of Fig. 12 would be rather surprising, because the Co monolayer interacts strongly with the W substrate and is expected to be ferromagnetic.[28] But due to the high coordination number in close-packed layers the lateral interactions will dominate the two-dimensional electronic bands and ferromagnetism will mainly cause a constant exchange splitting of majority and minority bands, so that a qualitative comparison should be possible.

Indeed, the dispersions of the d_{yz}- and d_{xz}-like bands 1 and 2 in Fig. 12 for 1-ML hcp Co/W(110) are, in general, similar to those in Fig. 16 at about 0.45-eV higher energy (flat for odd bands, large and downwards around $\bar{\Gamma}$ for even bands), but the d_{xz} and d_{yz} states at $\bar{\Gamma}$ are not degenerated as required by group theory for hexagonal symmetry. Obviously, the electronic structure of the Co monolayer is disturbed by its distortion (see Sec. III A) and by the underlying substrate C_{2v} symmetry. The observed shift of the d_{xz} to higher and of the d_{yz} band to lower E_B at $\bar{\Gamma}$ explains the crossing of bands 1 and 2 (Fig. 12) along $[1\bar{1}0]_W$.

For the parabolalike even bands around $\bar{M}$ in Fig. 12, there are two possible explanations. The first one is that they are the two even bands (crosses) of Fig. 16 which end at E_F (d-like) and 2.8 eV above E_F (s-like) at $\bar{M}$.[27] The second one would be an interpretation as an exchange splitting of the d-like band of about 0.6 eV at $\bar{M}$. Other possible exchange-split states can be found at $\bar{\Gamma}$, where weak d_{yz} states are 0.83 eV below the dominating d_{yz} band 1 (Fig. 12, Table I). Compared to the calculated

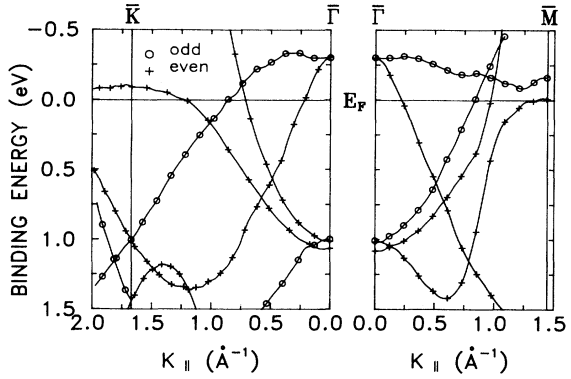

FIG. 16. Calculated paramagnetic band structure (Ref. 27) for an unsupported hexagonal monolayer of Co. Even and odd bands with respect to the $\bar{\Gamma}\bar{K}$ and $\bar{\Gamma}\bar{M}$ mirror planes are marked by crosses and circles, respectively. From top to bottom the bands are d_{xz}- and d_{yz}-like (degenerated), d_{xy}- and $d_{x^2-y^2}$-like (degenerated), and $d_{3z^2-r^2}$-like at $\bar{\Gamma}$ (Ref. 27).

exchange splitting of the bcc monolayer [1.2 eV at $\bar{\Gamma}$, 1.0 eV at $\bar{N}$ (Ref. 25)] this reduction to about 0.8 eV at $\bar{\Gamma}$ and 0.6 eV at $\bar{M}$ appears rather large. However, theoretical predictions[29] give similar trends connected with increasing d-orbital overlap.

C. The electronic structure of thicker films

We now turn to the electronic structure of Co films with two and more hcp(0001) layers thickness. For the double layer a shift of the d_{xz} band (Table I, circles in Figs. 12 and 13) and broad structures (Fig. 6) were observed at $\bar{\Gamma}$. The increased number of Co atoms in the two-dimensional unit cell increases also the number of electronic states. This is observable too for the third Co layer, where a new sharp band close to E_F and symmetric to $\bar{M}$ appears, visible already for 2.3 ML in Fig. 13. The split odd bands which exist in the double layer are better resolved than comparable states in the Ni/W(110) system,[9] but the antibonding band which was clearly observed in this system is not seen in Co, probably because it is located above E_F.

A comparison of many series similar to Fig. 10 shows for the $[1\bar{1}0]_W$ azimuth that the He I spectra qualitatively do not change much above 4 ML. They are dominated from there by three-dimensional direct transitions, as is Ni on W(110).[30] In this respect the surprising similarity between the dispersions of the dominating odd split bands in the double layer (Fig. 13) and in thick films (Fig. 14) reveals that the lateral interaction within the close-packed Co layers is an important factor governing the shape of these bands.

A comparison with photoemission experiments of Co single-crystal (0001) faces shows, in general, good agreement in the normal emission peak positions between the 12-ML-thick film (Table I) and the bands of Ref. 31 which are accessible with $h\nu = 21.22$ eV. In detail they differ: our strongest peak at $E_B = 0.64$ eV is only a weak structure for $h\nu < 21$ eV (Ref. 31) and is not visible in the He I spectra of Ref. 32. The sharp feature at E_F [Fig. 10(b)] is observed in Ref. 31 only as a weak shoulder at

$h\nu=21$ eV.

These intensity differences can be attributed only in part to different angles of incidence of the light and to the poorer angular resolution in the previous studies. The strong difference between the spectra taken with *s*- and *p*-polarized light (Fig. 6, 8 ML) is, however, unexpected in normal emission geometry on C_{6v} and C_{3v} crystal faces, because single group theory predicts degeneration of even and odd states at $\bar{\Gamma}$.

D. Comparison with other systems

It is interesting to compare the ps and cp monolayer results for Co with those of its neighbor in the periodic system Ni which forms the same monolayer structures on W(110), but is presumably paramagnetic. Upon the ps-to-cp transition, the d_{xz} overlap increases largely as a result of the increase in packing density along $[001]_W$, and along the same direction the band shape changes very much, both for Co and Ni,[9] respectively. For Co the bands 2 in Figs. 11 and 12 significantly differ in their shape also along $[1\bar{1}0]_W$ and in their binding energy at $\bar{\Gamma}$ (Table I), but for Ni the corresponding bands are very similar and only increase in intensity.[9] The reason for this difference between elements with similar electronic configuration may be sought in the interfacial character of the band 2*b* of the ps Co monolayer,[25] thus in the difference of the film-substrate interaction between Co and Ni on W(110).

A rigid shift of the calculated band structure for the unsupported hexagonal Ni monolayer[27] by 0.73 eV to higher E_B, justified by the binding of the monolayer to the W substrate in connection with charge redistribution, gives quite good agreement along $\bar{\Gamma}\bar{M}$ with the experimental data for the hexagonal Ni monolayer on W(110).[9] Both for Co and Ni on W(110) the d_{xz} and d_{yz} bands are not degenerated at $\bar{\Gamma}$, but are shifted in opposite directions in the two metals and thus cross along $\bar{\Gamma}\bar{M}$ for Co and along $\bar{\Gamma}\bar{K}$ for Ni.[9]

On other substrates, layer-by-layer growth of hcp(0001) Co has also been reported for Cu(111).[33] At $h\nu=25$ eV and 1 ML the normal emission ARUPS peak is rather broad; at two layers it already resembles the bulk peak form. The authors concluded that the exchange splitting ΔE_{exch} of the monolayer at $\bar{\Gamma}$ and $\bar{K}$ is 0.7 and 0.5 eV, respectively. These values are close to those proposed in Sec. IV B for the cp monolayer on W(110). Recent measurements, however, give an exchange splitting of 1.05 eV independent of Co film thickness on Cu(111) and indicate initial bilayer instead of monolayer growth.[34] According to theoretical predictions[6] and AES measurements,[35] however, the growth mode of Co on Cu(111) is still an open question.

Co on Cu(001) forms metastable fcc(001) layers.[36] For the monolayer $\Delta E_{\text{exch}}=0.8$ eV was reported,[37] whereas calculations for thicker "face-centered-tetragonal layers"[38] yield $\Delta E_{\text{exch}}=1.3$ eV. Other calculations for Co on Ag(001) yield similar high values.[28,29] The monolayer and double-layer photoemission spectra of Co on Au(001) (Ref. 39) are almost structureless.

V. SUMMARY AND CONCLUSIONS

The pseudomorphic (bcc) and the close-packed ("hcp") monolayers of Co on W(110) have narrow *d* bands, similar to Ni on W(110). Dissimilar to Ni, in which the dominating bands are located 0.65 eV below E_F, they are within 0.2 eV of E_F in the case of Co. A comparison with band-structure calculations for a bcc Co monolayer on W(110) allows us to identify them as minority bands. The majority bands are displaced by exchange splitting 1.2 and 1.0 eV downward at the $\bar{\Gamma}$ and $\bar{N}$ points, respectively, where they overlap with a region of high W 5*d* density of states. Due to the resulting delocalization they could not be observed. The results indicate a smaller exchange splitting in the cp monolayer, 0.85 and 0.6 eV at the $\bar{\Gamma}$ and $\bar{M}$ points, respectively. As judged by the spectra, the electronic structure of the close-packed monolayer differs significantly from the pseudomorphic layer in the case of Co, but not in the case of Ni on W(110). Band-structure calculations are needed for a detailed discussion.

The influence of symmetry and packing density is seen in the difference between ps and cp monolayers; the influence of film-substrate interaction is evident in the formation of an interface state in the ps Co monolayer on W(110) and in the comparison of the cp monolayer with the double layer on W(110) and on Cu(111). A factor which appears to be important for the shape and location of the major bands in close-packed layers is the lateral interaction. This follows from a comparison of the bands in the $\bar{\Gamma}\bar{M}$ direction (parallel $[1\bar{1}0]_W$) in which the periodicity of film and substrate is very similar. As a result the bands of the cp monolayer on W(110) are comparable to those of an unsupported monolayer, and the bands of the double layer already are similar to those of thick films. In contrast, the bands change strongly with the ps-to-cp transition along the direction with large misfit ($[001]_W$), the $\bar{\Gamma}\bar{K}$ direction.

The results reported here not only give a detailed picture of the evolution of the electronic structure with film thickness but also show the usefulness of UPS for the evaluation of the structure and perfection of the layers. The perfection is seen in the sharpness and intensity of the bands, in particular in the submonolayer range and up to about 3 ML. The spectra from the 12-ML-thick film are as sharp or sharper than those from bulk Co(0001) single-crystal surfaces. Above 4–5 ML little change is seen in the spectra so that bulk surface properties are to be expected from this thickness on upward in agreement with chemisorption studies. Below this thickness the changes of the electronic structure allow us to select characteristic energies at which the UPS intensities are very sensitive to structural changes, for example from bcc to hcp packing, and—upon closer inspection—to the layer growth: linear segments corresponding to successive monolayers appear. The rounding of the transitions between them gives information on deviations from perfect layer growth. Thus, UPS gives information similar to and sometimes even better than AES.

ACKNOWLEDGMENTS

This work was supported in part by the Volkswagen Foundation (Hannover), in part by the Deutsche Forschungsgemeinschaft. The authors wish to thank B. Weimert, J. Noffke, and L. Fritsche for the detailed band-structure results, and also G. Lilienkamp, M. Jałochowski, and Y. Fuwa for experimental cooperation as well as P. Cyris for the preparation of the W sample.

[1]U. Gradmann, in *Handbook of Ferromagnetic Materials,* edited by K. H. J. Buschow (Elsevier, Amsterdam, 1993), Vol. 7, p. 1.
[2]C. T. Campbell, Ann. Rev. Phys. Chem. **41**, 775 (1990).
[3]D. E. Eastman and W. D. Grobman, Phys. Rev. Lett. **30**, 177 (1973).
[4]K. Jacobi, in *Angle-Resolved Photoemission,* edited by S. D. Kevan (Elsevier, Amsterdam, 1992), Vol. 74, p. 37.
[5]E. Bauer and J. H. van der Merwe, Phys. Rev. B **33**, 3657 (1986).
[6]J. H. van der Merwe and E. Bauer, Phys. Rev. B **39**, 3632 (1989).
[7]J. Kołaczkiewicz and E. Bauer, Surf. Sci. **144**, 495 (1984).
[8]M. Tikhov and E. Bauer, Surf. Sci. **232**, 73 (1990).
[9]C. Koziol, G. Lilienkamp, and E. Bauer, Phys. Rev. B **41**, 3364 (1990).
[10]G. Lilienkamp, C. Koziol, and E. Bauer, Surf. Sci. **226**, 358 (1990).
[11]G. Lilienkamp, Ph.D. thesis, TU Clausthal, 1990.
[12]G. Lilienkamp, C. Koziol, and E. Bauer, in *Reflection High-Energy Electron Diffraction and Reflection Electron Imaging of Surfaces,* edited by P. K. Larsen and P. J. Dobson (Plenum, New York, 1988), p. 489.
[13]K. Jacobi, P. Geng, and W. Ranke, J. Phys. E. **11**, 982 (1978).
[14]B. G. Johnson, P. J. Berlowitz, D. W. Goodman, and C. H. Bartholomew, Surf. Sci. **217**, 13 (1989).
[15]J. G. Ociepa, P. J. Schultz, K. Griffiths, and P. R. Norton, Surf. Sci. **225**, 281 (1990).
[16]C. M. Wei, T. C. Zhao, and S. Y. Tong, Phys. Rev. Lett. **65**, 2278 (1990).
[17]C. M. Wei, T. C. Zhao, and S. Y. Tong, Phys. Rev. B **43**, 6354 (1991).
[18]S. Y. Tong (private communication).
[19]J. H. van der Merwe and E. Bauer (unpublished).
[20]B. C. Bolding and E. A. Carter, Phys. Rev. B **44**, 3251 (1991).
[21]A. Pavlovska and E. Bauer, Surf. Sci. **177**, 473 (1986).
[22]F. J. Himpsel and D. E. Eastman, Phys. Rev. B **20**, 3217 (1979).
[23]A. Goldmann, Vak. Tech. **31**, 204 (1982).
[24]J. E. Houston, P. J. Feibelman, D. G. O'Neill, and D. R. Hamann, Phys. Rev. B **45**, 1811 (1992).
[25]B. Weimert, J. Noffke, and L. Fritsche (private communication).
[26]E. Wimmer, H. Krakauer, M. Weinert, and A. J. Freeman, Phys. Rev. B **24**, 864 (1981).
[27]E. Wimmer, J. Phys. F **14**, 2613 (1984).
[28]S. Blügel, B. Drittler, R. Zeller, and P. H. Dederichs, Appl. Phys. A **49**, 547 (1989).
[29]S. Blügel, Phys. Rev. Lett. **68**, 851 (1992).
[30]K.-P. Kämper, W. Schmitt, G. Güntherodt, and H. Kuhlenbeck, Phys. Rev. B **38**, 9451 (1988).
[31]F. J. Himpsel and D. E. Eastman, Phys. Rev. B **21**, 3207 (1980); D. E. Eastman, F. J. Himpsel, and J. A. Knapp, Phys. Rev. Lett. **44**, 95 (1980).
[32]P. Heimann, E. Marschall, H. Neddermeyer, M. Pessa, and H. F. Roloff, Phys. Rev. B **16**, 2575 (1977).
[33]L. Gonzalez, R. Miranda, M. Salmerón, J. A. Vergés, and F. Ynduráin, Phys. Rev. B **24**, 3245 (1981); R. Miranda, F. Ynduráin, D. Chandesris, J. Lecante, and Y. Petroff, Surf. Sci. **117**, 319 (1982); Phys. Rev. B **25**, 527 (1982).
[34]G. J. Mankey, R. F. Willis, and F. J. Himpsel, Phys. Rev. B **47**, 190 (1993).
[35]M. Tikhov and E. Bauer (unpublished).
[36]Hong Li and B. P. Tonner, Surf. Sci. **237**, 141 (1990).
[37]R. Miranda, D. Chandesris, and J. Lecante, Surf. Sci. **130**, 269 (1983).
[38]C. M. Schneider, P. Schuster, M. Hammond, H. Ebert, J. Noffke, and J. Kirschner, J. Phys. Condens. Matter **3**, 4349 (1991).
[39]W. Heinen, C. Carbone, T. Kachel, and W. Gudat, J. Electron. Spectrosc. Relat. Phenom. **51**, 701 (1990).